Correspondence

Two Parallel Single-Gimbal Control Moment Gyros Actuated Spacecraft Attitude Maneuver

This correspondence investigates the underactuated spacecraft attitude maneuver problem using two parallel single-gimbal control moment gyros (SGCMGs). According to the configuration of the SGCMGs, the principle axes of the spacecraft are divided into two parts, namely, the axes with and without direct control input. Based on this division, a two-level control strategy, a low-level tracking control part to track the desired angular velocity error about the axes with direct control input and a high-level sliding mode control part to stabilize the angular velocity error, is developed. Four numerical scenarios are conducted to verify the proposed control logic. Simulation results show that the target attitude is a global equilibrium and any attitude can be reached when the whole system is feasible. If the controllability is not satisfied, the spacecraft rotates in the adjacent region around the desired attitude.

I. INTRODUCTION

Recent space missions, such as the deep space exploration, put forward higher requirement to the spacecraft attitude control system. To enhance reliability, ensure survivability, and maintain the required performance, various robust controllers [1], [2] and fault-tolerant control strategies have been proposed [3], [4]. Existing fault-tolerant control strategies can be generally divided into passive ones [5] and active ones [6]. However, the foundation of both methods is the existence of system redundancies [7]. When the systems lose redundancy, existing fault-tolerant control strategies will be invalid. Even worse, when the number of actuators is less than that of system configuration variables, the system will degrade to an underactuated system. The origin of underactuation is multiple: it can be natural due to dynamics of the systems under study or it can be artificial either by design or by deliberately removing actuators for the purpose of building low-cost systems or finally due to actuators' failure [8]. Thus, developing control strategy for underactuated system

Authors' addresses: Chengfei Yue is with the Institute of Space Science and Applied Technology, Harbin Institute of Technology, Shenzhen 518055, China, E-mail: (yuechengfei@hit.edu.cn); Fan Wu, Feng Wang, and Xibin Cao are with the Research Center of the Satellite Technology, Harbin Institute of the Technology, Harbin 150001, China, E-mail: (wufanhnb@126.com; wfhitsat@hit.edu.cn; xbcao@hit.edu.cn); Shen Qiang is with the School of Aeronautics and Astronautics, Shanghai Jiao Tong University, Shanghai 200240, China, E-mail: (qiang.shen@sjtu.edu.cn); Krishna Dev Kumar is with the Department of Aerospace Engineering, Ryerson University, Toronto, ON M5B 2K3, Canada, E-mail: (kdkumar@ryerson.ca). *(Corresponding author: Feng Wang.)*

to maintain partial or complete control performance has become an active field due to the advantages of enhancing reliability of attitude control system, simplifying collocation of actuators, reducing cost, economize energy, etc. [9]. However, the restriction on the control authority makes the control design for underactuated system rather complicated, for instance, the controllability is difficult to determine [8].

Crouch first investigated the controllability of the spacecraft attitude control system using nonlinear geometrical control theory and gave necessary and sufficient conditions [10]. Li *et al.* [11] gave a comprehensive survey on the moving mass control technology and proposed a hybrid system of moving mass and reaction wheels to achieve underactuated control in [12]. Boyer and Alamir [13] further investigated the controllability of two wheeled satellite and stated that the satellite with two reaction wheels and nonnull kinetic momentum is not controllable over the entire state space of the spacecraft attitudes. Bhat *et al.* [14] investigated the controllability of spacecraft attitude using control moment gyros (CMGs). It is reported that spacecraft is controllable using one or more CMGs and any two attitude states having the same angular momentum can be achieved from another one when the CMGs are suitably steered in spite of the presence of CMGs' singular configuration. The controllability guarantees the existence of CMG motion to drive the spacecraft to spin state or rest attitude. More specifically, when the angular momentum of the CMG-spacecraft system locates in the angular envelope of the CMG array, the spacecraft can be controlled to any rest attitude. Otherwise, the spacecraft can be controlled to a spin state. This sparked a surge of interest in spacecraft attitude control using CMGs, even the underactuated cases with one [15] or two CMGs [16].

Underactuated spacecraft attitude control using CMGs is rather complicated due to the obstacle of the underactuated system and the inherent nonlinearity and singularity of the CMGs. Tsiotras *et al.* [17] gave a review on the spacecraft control problem subject to actuator failures till 2000. It is reported that "complete attitude stabilization is not completely understood" and "no global stabilizing control law has been reported in the literature." Afterward, Gui *et al.* [18], [19]investigated the attitude stabilization problem of rigid spacecraft by two CMGs. In these works, the total angular momentum of the overall CMG-spacecraft system is assumed to be zero. Under such a restricted condition, the spacecraft dynamics can be simplified into a two-axis system, which is fully actuated and the attitude stabilization can be achieved. However, the assumption is definitely too conservative for the CMG-actuated system comparing to the controllability condition stated in [14], and the coupling of the system dynamics has not been sufficiently used. To overcome these drawbacks, the underactuated attitude stabilization using two parallel single-gimbal control moment gyros (SGCMGs) has been addressed and the attitude stabilization is completed when the angular momentum constraints is satisfied [20].

This correspondence aims to give a systematic closed-loop control solution to the rigid spacecraft actuated by two parallel SGCMGs when the controllability property of the CMG-spacecraft system is satisfied. Even if the initial angular momentum exceeds the momentum envelop of the CMG array, the spacecraft system is forced to rotate about a specific target axis in the adjacent region. This control objective is realized by a two-level control strategy. First, the angular velocity along the axis without direct input is set to be zero. An ideal angular velocity input is designed to stabilize the reduced relative kinematics. Then, an angular velocity tracking controller is proposed to track the desired angular velocity input. Second, a higher level sliding mode control law is proposed to stabilize the nonzero angular velocity with a sufficient utilization of the coupling effect of the relative dynamics. The underactuated control strategy presented in this correspondence can be considered as a fault-tolerant control strategy of a rigid spacecraft under an extreme scenario that only two parallel SGCMGs are available to provide control torque, and it could also be regarded as a solution to design a new spacecraft where only two parallel SGCMGs are adopted in order to reduce the cost. Comparing to existing results, including our previous work [20], the main contributions are summarized as follows.

1) The feasible orientation for the attitude maneuver rather than the attitude stabilization under the momentum conservation constraint is given. The feasibility of the orientation gives an index to determine whether the attitude maneuver of two parallel SGCMGs actuated spacecraft can be achieved with a rest state.

2) The target attitude is set to be a global attractor and the attitude maneuver is completed by a feedback strategy. When the target orientation is feasible, the spacecraft is forced to align with the given direction with a rest state. Otherwise, the spacecraft is forced to rotate along the target orientation in the adjacent region.

3) The underactuated attitude maneuver problem using two SGCMGs without additional conservative constraints, such as the zero total angular momentum assumption and zero angular velocity assumption, is investigated. The requirement of additional conservative constraints in existing underactuated control approaches in [9], [18] and [21] is eliminated by choosing the target attitude in the feasible orientation set and sufficiently using the coupling effect of the relative dynamics.

The rest of this correspondence is organized as follows. Section II presents the preliminaries. Section III addresses the controller design procedures step by step in three theorems. Section IV gives the steering law and numerical simulations. Finally, Section V concludes this correspondence.

II. PRELIMINARIES

A. Two Parallel SGCMGs

Two identical SGCMGs are adopted as the actuator. A constant speed rotor is mounted on the gimbal frame with
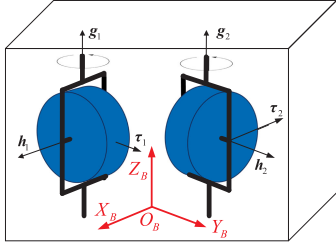
Fig. 1. Spacecraft with two parallel CMGs when $\delta_1 = 0$ and $\delta_2 = 0.5\pi$.

the gimbal axis denotes as $\hat{\boldsymbol{g}}$. The angular momentum of each SGCMG is h_0 along the axis $\hat{\boldsymbol{h}}$. The gyroscopic output $\boldsymbol{\tau} = -\dot{\delta}h_0\hat{\boldsymbol{t}}$ is along the axis $\hat{\boldsymbol{t}} = \hat{\boldsymbol{g}} \times \hat{\boldsymbol{h}}$ with $\dot{\delta}$ being the gimbal angular velocity. $\hat{\boldsymbol{g}}_i$, $\hat{\boldsymbol{h}}_i$, and $\hat{\boldsymbol{t}}_i$ form the CMG body coordinate $\mathcal{G}_i = \{\hat{\boldsymbol{g}}_i, \hat{\boldsymbol{h}}_i, \hat{\boldsymbol{t}}_i\}$ with the subscript i representing the ith CMG. The schematic diagram where the gimbals of both CMGs are aligned along the Z-axis of the spacecraft is shown in Fig. 1. Then, the angular moment of the CMGs $\boldsymbol{h}$ is modeled as [18]

$$\boldsymbol{h} = \begin{bmatrix} h_x \\ h_y \\ h_z \end{bmatrix} = h_0 \begin{bmatrix} \cos\delta_1 + \cos\delta_2 \\ \sin\delta_1 + \sin\delta_2 \\ 0 \end{bmatrix} \quad (1)$$

where $\delta_i (i = 1, 2)$ is the gimbal angle.

The magnitude of the angular momentum is

$$\|\boldsymbol{h}\| = h_0\sqrt{2 - 2\cos(\delta_1 - \delta_2)}. \quad (2)$$

Then, the angular momentum envelop of the CMGs in $\mathcal{F}_B$ is given as

$$\text{ENV}(\boldsymbol{h}) = \left\{ \boldsymbol{h} \,\middle|\, h_x^2 + h_y^2 = 4h_0^2, h_z = 0 \right\}. \quad (3)$$

As a momentum exchange device, $\dot{h}_z = h_z = 0$ from (1). Then, the direct control torques are limited in the X–Y plane and can be expressed by

$$\boldsymbol{\tau} = \begin{bmatrix} \tau_x \\ \tau_y \end{bmatrix} = -h_0 \begin{bmatrix} -\sin\delta_1 & -\sin\delta_2 \\ \cos\delta_1 & \cos\delta_2 \end{bmatrix} \begin{bmatrix} \dot{\delta}_1 \\ \dot{\delta}_2 \end{bmatrix} = -h_0 \boldsymbol{A}\dot{\boldsymbol{\delta}} \quad (4)$$

with matrix $\boldsymbol{A}$ being the Jacobian matrix.

From (4), it is clear that the matrix $\boldsymbol{A}$ loses rank when $\delta_2 - \delta_1 = k\pi (k \in \mathbb{Z})$ in which condition $\det(\boldsymbol{A}) = 0$. Physically, $\boldsymbol{h}$ is zero when k is odd and $\boldsymbol{h}$ achieves its maximum value $2h_0$ when k is even. These conditions correspond to the internal singularity and external singularity, respectively, [18], [22].

B. Spacecraft Attitude Dynamics and Kinematics

When the mass center of each CMG coincides with that of spacecraft and the kinetic energy caused by gimbal motion is ignored, the CMG-spacecraft system without the consideration of external disturbances and gimbal friction can be modeled as [23]

$$\boldsymbol{J}\dot{\boldsymbol{\omega}} = -\boldsymbol{\omega}^\times \boldsymbol{h}_t - \dot{\boldsymbol{h}} \quad (5)$$

where $\boldsymbol{J} = \text{diag}([J_x, J_y, J_z]) \in \mathbb{R}^{3\times3}$ represents the inertia matrix of the spacecraft, $\boldsymbol{\omega} \in \mathbb{R}^3$ is the angular velocity with respect to the inertial frame $\mathcal{F}_I$ and expressed in $\mathcal{F}_B$, and

$\boldsymbol{h}_t = \boldsymbol{J}\boldsymbol{\omega} + \boldsymbol{h}$ is the total angular momentum of spacecraft and CMG array. The operator $\boldsymbol{a}^\times$ generates a skew matrix to express the cross product of two vector as $\boldsymbol{a} \times \boldsymbol{b} = \boldsymbol{a}^\times\boldsymbol{b}$.

When the unit quaternion $\boldsymbol{Q} = [q_0, \ q_1, \ q_2, \ q_3]^T = [q_0, \ \boldsymbol{q}_v^T]^T \in \mathbb{R}^4$, with q_0 and $\boldsymbol{q}_v$ being the scalar and vector part of $\boldsymbol{Q}$, respectively, and satisfying $q_0^2 + \boldsymbol{q}_v^T\boldsymbol{q}_v = 1$, describes the orientation of $\mathcal{F}_B$ with respect to $\mathcal{F}_I$, we have

$$\dot{\boldsymbol{Q}} = \begin{bmatrix} \dot{q}_0 \\ \dot{\boldsymbol{q}}_v \end{bmatrix} = \frac{1}{2} \begin{bmatrix} -\boldsymbol{q}_v^T \\ q_0\boldsymbol{I}_3 + \boldsymbol{q}_v^\times \end{bmatrix} \boldsymbol{\omega}. \quad (6)$$

The transformation matrix $\boldsymbol{R}$ from $\mathcal{F}_I$ to $\mathcal{F}_B$ can be expressed by $\boldsymbol{Q}$ as $\boldsymbol{R}(\boldsymbol{Q}) = (q_0^2 - \boldsymbol{q}_v^T\boldsymbol{q}_v)\boldsymbol{I}_3 + 2\boldsymbol{q}_v\boldsymbol{q}_v^T - 2q_0\boldsymbol{q}_v^\times$.

C. Relative Attitude Error Dynamics and Kinematics

The quaternion error $\boldsymbol{Q}_e = [e_0, \boldsymbol{e}_v^T]^T \in \mathbb{R}^4$ describing the discrepancy between the actual unit-quaternion $\boldsymbol{Q}$ and the target unit-quaternion $\boldsymbol{Q}_d$ is given by

$$\boldsymbol{Q}_e = \boldsymbol{Q}_d^{-1} \circ \boldsymbol{Q} \quad (7)$$

where $\boldsymbol{Q}_d^{-1}$ is the conjugate quaternion of $\boldsymbol{Q}_d$ and "$\circ$" represents the quaternion multiplication.

Then, the error quaternion kinematics is given as [24]

$$\dot{\boldsymbol{Q}}_e = \begin{bmatrix} \dot{e}_0 \\ \dot{\boldsymbol{e}}_v \end{bmatrix} = \frac{1}{2} \begin{bmatrix} -\boldsymbol{e}_v^T \\ e_0\boldsymbol{I}_3 + \boldsymbol{e}_v^\times \end{bmatrix} \boldsymbol{\Omega} \quad (8)$$

with $\boldsymbol{\Omega} = \boldsymbol{\omega} - \boldsymbol{R}^T(\boldsymbol{Q}_e)\boldsymbol{\omega}_d$.

For the attitude maneuver, the target angular velocity $\boldsymbol{\omega}_d$ is required to be zero. Substituting $\boldsymbol{\Omega}$ into (5) with $\tau_x = -\dot{h}_x$, $\tau_y = -\dot{h}_y$, and expanding the equation, the relative error dynamics is given by

$$\begin{cases} J_x\dot{\Omega}_x = (J_y - J_z)\Omega_y\Omega_z + \Omega_z h_y + \tau_x \\ J_y\dot{\Omega}_y = (J_z - J_x)\Omega_x\Omega_z - \Omega_z h_x + \tau_y \\ J_z\dot{\Omega}_z = (J_x - J_y)\Omega_x\Omega_y + \Omega_y h_x - h_y\Omega_x \end{cases} \quad (9)$$

D. Problem Statement

Since CMGs are momentum exchange device and the external torque acting on the spacecraft is assumed to be zero, the angular momentum in frame $\mathcal{F}_I$ is conserved, which states that the initial angular momentum of the CMG-spacecraft system should be equal to that of the CMG array when the angular velocity of the spacecraft is stabilized at the target attitude

$$\boldsymbol{R}(\boldsymbol{Q}_0)^T\boldsymbol{h}_t(t_0) = \boldsymbol{R}(\boldsymbol{Q}_d)^T\boldsymbol{h}_t(t_f) \quad (10)$$

with $\boldsymbol{Q}_0$ being the initial attitude, t_0 and t_f being the initial and final time instant, respectively.

For the spacecraft system, the following property holds:

$$\boldsymbol{R}(\boldsymbol{Q}_0)\boldsymbol{R}(\boldsymbol{Q}_d)^T = \boldsymbol{R}(\boldsymbol{Q}_d^{-1} \circ \boldsymbol{Q}_0) = \boldsymbol{R}(\boldsymbol{Q}_e) \quad (11)$$

using (7).

Substituting the relationship $\boldsymbol{h}_t = \boldsymbol{J}\boldsymbol{\omega} + \boldsymbol{h}$ into (10), we have

$$\boldsymbol{R}(\boldsymbol{Q}_e(t_0))^T\boldsymbol{h}_t(t_0) = \boldsymbol{J}\boldsymbol{\omega}(t_f) + \boldsymbol{h}(t_f). \quad (12)$$

Then, the final angular velocity can be solved as

$$\boldsymbol{\omega}(t_f) = \boldsymbol{J}^{-1}\left\{[\boldsymbol{R}(\boldsymbol{Q}_e(t_0))^T\boldsymbol{h}_t(t_0)] - \boldsymbol{h}(t_f)\right\}. \quad (13)$$
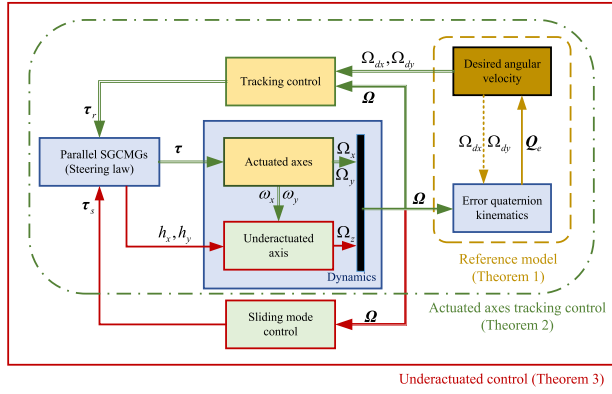
Fig. 2.   Overall control strategy.

For a complete attitude maneuver, $\omega(t_f)$ is required to be zero. As a consequence, we require the initial condition of $\boldsymbol{R}(\boldsymbol{Q}_e(t_0))^T\boldsymbol{h}_t(t_0)$ to be within the momentum envelope of the SGCMG array, which means we can always find a combination of gimbal angle such that the total angular momentum of the SGCMG array is equal to the initial angular momentum of the spacecraft bus. Then, the total angular momentum can be transferred to or absorbed by the SGCMGs. This results in the following definition.

DEFINITION 1 For the initial attitude $\boldsymbol{Q}_0$ and target attitude $\boldsymbol{Q}_d$, when the state of $\boldsymbol{R}(\boldsymbol{Q}_d)\boldsymbol{R}(\boldsymbol{Q}_0)^T\boldsymbol{h}_t(t_0)$ locates within the momentum envelop expressed in (3) [$\boldsymbol{R}(\boldsymbol{Q}_d)\boldsymbol{R}(\boldsymbol{Q}_0)^T\boldsymbol{h}_t(t_0) \in$ ENV($\boldsymbol{h}$)], the combination of $\boldsymbol{Q}_0$ and $\boldsymbol{Q}_d$ is called a feasible orientation combination for the configured SGCMGs.

This correspondence aims to provide an attitude controller to complete the attitude maneuver from $\boldsymbol{Q}_0$ to $\boldsymbol{Q}_d$ when they are a feasible combination. In contrast, when the attitude is not feasible, the spacecraft is forced to rotate around the target attitude in the adjacent region.

III.   CONTROLLER DESIGN

In this section, a novel attitude controller is designed to achieve the attitude reorientation. Before describing the main results, the following lemmas are needed.

LEMMA 1 For any positive definite symmetric inertia matrix $\boldsymbol{J}$, the energylike function $\boldsymbol{x}^T\boldsymbol{J}\boldsymbol{x}$ is both lower and upper bounded as $\underline{J}\|\boldsymbol{x}\|^2 \le \boldsymbol{x}^T\boldsymbol{J}\boldsymbol{x} \le \overline{J}\|\boldsymbol{x}\|^2$ $\forall \boldsymbol{x} \in \mathbb{R}^3$ with $\underline{J} \in \mathbb{R}^+$ and $\overline{J} \in \mathbb{R}^+$ [25]. Also, there always exists a parameter λ, such that $\boldsymbol{J}\boldsymbol{x} \le \lambda\|\boldsymbol{x}\|$.

LEMMA 2 For any real number $\alpha \in \mathbb{R}^+$, $\beta \in \mathbb{R}^+$ and $0 < \gamma < 1$, an extended Lyapunov condition of finite-time stability can be given in the form of fast terminal sliding mode as $\dot{V}(\boldsymbol{x}) + \alpha V(\boldsymbol{x}) + \beta V^\gamma(\boldsymbol{x}) \le 0$, and the settling time can be estimated by $t_s \le \frac{1}{\alpha(1-\gamma)} \ln \frac{\alpha V^{1-\gamma}(x_0)+\beta}{\beta}$ [26].

The novel controller consists of two parts, i.e., a low-level tracking control part that tracks the desired angular velocity error about the actuated axes and a high-level sliding mode control part that stabilizes the overall system in finite time. The control structure is shown Fig. 2. First,

the desired angular velocity errors Ω_{dx} and Ω_{dy} stabilize the error quaternion kinematics (14) when Ω_{dz} is set to be zero. This part can be regarded as a reference model and is circled by brown dashed line in Fig. 2. To track the desired angular velocity error, a tracking control part $\boldsymbol{\tau}_r$ is designed to drive the actuated axes. This part is circled by dark green dot dashed line. The stability of the desired angular velocity error and the tracking error is given in Theorems 1 and 2, and the corresponding result forms the low-level tracking control. To control the under-actuated axis, the coupling effect caused by Ω_x, Ω_y, h_x, and h_y on the underactued axis is used and a higher level sliding mode control $\boldsymbol{\tau} = \boldsymbol{\tau}_r + \boldsymbol{\tau}_s$ containing the tracking control part $\boldsymbol{\tau}_r$ and sliding mode control part $\boldsymbol{\tau}_s$ is designed. Finite-time stabilization of the sliding vector is proved by Theorem 3. Then, the underactuated attitude maneuver circled by red line in Fig. 2 is completed under the overall control torque $\boldsymbol{\tau}$.

A.   Low-Level Tracking Control

1) *Reference Model:* For the system (8), it can be rewritten as

$$\begin{bmatrix}\dot{e}_0\\\dot{e}_1\\\dot{e}_2\\\dot{e}_3\end{bmatrix} = \frac{1}{2}\begin{bmatrix}-e_1 & -e_2\\e_0 & -e_3\\e_3 & e_0\\-e_2 & e_1\end{bmatrix}\begin{bmatrix}\Omega_{dx}\\\Omega_{dy}\end{bmatrix} + \begin{bmatrix}-e_3\\e_2\\-e_1\\e_0\end{bmatrix}\Omega_{dz}. \quad (14)$$

Since there is no direct control torque on the Z-axis, we set the desired angular velocity error Ω_{dz} to be zero in this section and design the desired angular velocity errors Ω_{dx} and Ω_{dy} to stabilize the reference model, i.e., the inner loop circled by brown dashed line in Fig. 2.

To stabilize the kinematics (14) with $\Omega_{dz} = 0$, a desired velocity input is given by

$$\Omega_{dx} = \begin{cases}-k_1 e_1 + k_2 \dfrac{e_2 e_3}{\mathbf{e}_v{}^T \mathbf{e}_v} & \|\mathbf{e}_v\| \ne 0\\ 0 & \|\mathbf{e}_v\| = 0\end{cases}$$

$$\Omega_{dy} = \begin{cases}-k_1 e_2 - k_2 \dfrac{e_1 e_3}{\mathbf{e}_v{}^T \mathbf{e}_v} & \|\mathbf{e}_v\| \ne 0\\ 0 & \|\mathbf{e}_v\| = 0\end{cases} \quad (15)$$

where $k_1 \in \mathbb{R}^+$, $k_2 \in \mathbb{R}^+$, and $k_2 > 2k_1$.

THEOREM 1 Consider the kinematics in (14) and let the input Ω_{dx} and Ω_{dy} be the desired velocity in (15). For any initial condition satisfying $e_1^2 + e_2^2 \ne 0$, the following properties hold:

1) the desired velocities Ω_{dx} and Ω_{dy} are bounded;
2) $\boldsymbol{e}_v = 0$ is an almost global attractor and $\boldsymbol{e}_v \to 0$ as $t \to \infty$;
3) Ω_{dx} and Ω_{dy} converge to zero as $t \to \infty$.

PROOF

1) Since $|e_1 e_3| \le \frac{1}{2}(e_1^2 + e_3^2) \le \frac{1}{2}\boldsymbol{e}_v^T\boldsymbol{e}_v$, and the unit quaternion is constrained by $\|\boldsymbol{Q}_e\| = 1$, we have $|\Omega_{dx}| \le k_1 + \frac{1}{2}k_2$. Similarly, the upper bound of Ω_{dy} is also given as $|\Omega_{dy}| \le k_1 + \frac{1}{2}k_2$.

2) When $\|e_v\| = 0$, $\Omega_{dx} = \Omega_{dy} = 0$ and $\dot{e}_v = 0$. The property of $e_v \to 0$ is naturally satisfied. When $\|e_v\| \neq 0$, substituting Ω_{dx} and Ω_{dy} into (14), one obtains $\dot{e}_3 = -\frac{k_2}{2}\frac{e_1^2+e_2^2}{e_v^T e_v}e_3$. Furthermore, an energylike function is chosen as $V_0 = e_3^2/(e_1^2 + e_2^2)$ when $e_1^2 + e_2^2 \neq 0$. The time derivative is given as $\dot{V}_0 = -k_2 \frac{e_3^2}{e_v^T e_v} - \frac{e_3^2(k_2 e_3^2 - k_1 e_0 e_v^T e_v)}{e_v^T e_v (e_1^2 + e_2^2)} = -k_2 \frac{e_3^2}{e_1^2+e_2^2} + k_1 e_0 \frac{e_3^2}{e_1^2+e_2^2} \leq -k_2 \frac{e_3^2}{e_1^2+e_2^2} + k_1 \frac{e_3^2}{e_1^2+e_2^2} = -(k_2 - k_1)V_0$ with $|e_0| \leq 1$. Thus, one obtains $V_0(t) \leq V_0(0)e^{-(k_2-k_1)t}$, which leads to $0 \leq e_3^2 \leq (e_1^2 + e_2^2)V_0(t) \leq V_0(0)e^{-(k_2-k_1)t}$. Thus, $e_3(t)$ goes to zero faster than $e_1^2 + e_2^2$. Similarly, one obtains $\dot{e}_0 = \frac{1}{2}(e_1^2 + e_2^2)$. Then, e_0 increases until the constraint $e_0 = 1$ is achieved. Then, by the unit constraint of quaternion error Q_e, $e_1 \to 0$ and $e_2 \to 0$ as $t \to \infty$. To show that $e_v = 0$ is an almost global attractor, the Lyapunov candidate is chosen as $V_1 = (1 - e_0)^2 + e_v^T e_v$. The time derivative is given by $\dot{V}_1 = e_v^T \Omega = -k_1(e_1^2 + e_2^2) \leq 0$. Thus, $V_1 \to 0$ gradually. Since e_v is a unique equilibrium, it is a global attractor.

3) When e_v converges to zero, the e_v related functions Ω_{dx} and Ω_{dy} go to zero naturally. ∎

2) *Actuated Axes Tracking Control:* To render the velocity Ω to track the proposed velocity in (15) regardless of Ω_z, i.e., to stabilize the middle loop circled by dark green dot dashed line in Fig. 2, an angular velocity tracking controller is given by

$$\tau_r = \begin{bmatrix} \tau_{rx} \\ \tau_{ry} \end{bmatrix} = \begin{bmatrix} -a_1 - k_3 J_x \tilde{\Omega}_x + J_x \dot{\Omega}_{dx} \\ -a_2 - k_3 J_y \tilde{\Omega}_y + J_y \dot{\Omega}_{dy} \end{bmatrix} \quad (16)$$

with $a_1 = (J_y - J_z)\Omega_y\Omega_z + \Omega_z h_y$, $a_2 = (J_z - J_x)\Omega_x\Omega_z - \Omega_z h_x$, $\tilde{\Omega}_x = \Omega_x - \Omega_{dx}$, and $\tilde{\Omega}_y = \Omega_y - \Omega_{dy}$. In (16), $\dot{\Omega}_{dx}$ and $\dot{\Omega}_{dy}$ can be obtained by taking time derivative of equation (15) when $\|e_v\| \neq 0$, and it is set to be zero when $\|e_v\| = 0$.

THEOREM 2 Consider the X and Y axes of system (9) with direct control input and let the control command be (16). $\Omega_x = \Omega_{dx}$ and $\Omega_x = \Omega_{dy}$ are global exponentially stable equilibrium, and Ω_x and Ω_y converge to Ω_{dx} and Ω_{dy} exponentially.

PROOF Consider a Lyapunov candidate in the form of

$$V_2 = \frac{1}{2}\chi^T J^\dagger \chi \quad (17)$$

with $\chi = [\tilde{\Omega}_x, \tilde{\Omega}_y]^T$, and $J^\dagger = \text{diag}([J_x, J_y])$.

Taking the time derivative of V_2 and substituting (16), one obtains

$$\dot{V}_2 = \chi^T J^\dagger \dot{\chi} = \tilde{\Omega}_x J_x (\dot{\Omega}_x - \dot{\Omega}_{dx}) + \tilde{\Omega}_y J_y (\dot{\Omega}_y - \dot{\Omega}_{dy})$$
$$= -k_3 J_x \tilde{\Omega}_x^2 - k_3 J_y \tilde{\Omega}_y^2 = -k_3 V_2 \leq 0. \quad (18)$$

Thus, $V_2(t) = V_2(0)e^{-k_3 t}$.

Applying Lemma 1 to the Lyapunov candidate V_2, one can conclude that $\Omega_x = \Omega_{dx}$ and $\Omega_x = \Omega_{dy}$ are global exponential equilibrium according to the exponential stability theorem [27]. Simultaneously, one concludes that Ω_x and Ω_y converge to Ω_{dx} and Ω_{dy} exponentially under the controller in (16). ∎

B. High-Level Sliding Mode Underactuated Control

For the underactuated Z-axis, although Ω_z cannot be controlled directly by a torque about the Z axis, it can be controlled through its nonlinear coupling with the transverse rates Ω_x and Ω_y and through the coupling effect produced by the CMG momentum h_x and h_y, as shown in (1). To stabilize $\Omega_z = 0$ and achieve an overall system stabilization, i.e., the outer loop circled by red in Fig. 2, a sliding mode surface, which is a linear combination of Ω_z and $\dot{\Omega}_z$, is given by

$$s = k_4 \Omega_z + \dot{\Omega}_z \quad (19)$$

with $k_4 \in \mathbb{R}^+$.

A sliding mode controller is designed as

$$\tau = \tau_s + \tau_r \quad (20a)$$
$$\tau_s = -\left(k_5 s + k_6 \text{sgn}(s)\right) \Lambda^+ \quad (20b)$$

with $k_5 \in \mathbb{R}^+$, $k_6 = |\Phi| + k_7$, $k_7 \in \mathbb{R}^+$, and "sgn" is the signum function. The remaining parameters are given by

$$\Lambda = \begin{bmatrix} (c\alpha_1 - \alpha_3)\Omega_y - \alpha_3\alpha_1 h_y \\ (c\alpha_2 + \alpha_3)\Omega_x + \alpha_3\alpha_2 h_x \end{bmatrix} \quad (21)$$

with $\alpha_1 = 1/J_x$, $\alpha_2 = 1/J_y$, $\alpha_3 = 1/J_z$, and $c = (J_x - J_y)/J_z$, and

$$\Phi(\bullet) = ck_4\Omega_x\Omega_y + \alpha_3 k_4 h_x\Omega_y - \alpha_3 k_4 h_y\Omega_x - ck_3\tilde{\Omega}_x\Omega_y$$
$$- ck_3\tilde{\Omega}_y\Omega_x + c\dot{\Omega}_{dx}\Omega_y + c\dot{\Omega}_{dy}\Omega_x - \alpha_3 k_3\tilde{\Omega}_y h_x$$
$$+ \alpha_3 k_3\tilde{\Omega}_x h_y + \alpha_3\dot{\Omega}_{dy}h_x - \alpha_3\dot{\Omega}_{dx}h_y$$
$$- \alpha_3 J_x\Omega_y\dot{\Omega}_{dx} + \alpha_3 k_3 J_x\Omega_y\tilde{\Omega}_x + \alpha_3 J_y\Omega_x\dot{\Omega}_{dy}$$
$$- \alpha_3 k_3 J_y\Omega_x\tilde{\Omega}_y + \alpha_3 a_1\Omega_y - \alpha_3 a_2\Omega_x \quad (22)$$

and the operator x^+ is given by

$$x^+ = \begin{cases} \dfrac{x}{x^T x} & \|x\| \neq 0 \\ 0 & \|x\| = 0 \end{cases}. \quad (23)$$

COROLLARY 1 Consider Λ defined in (21), and let the controller be (20), the set $\{\Lambda | \Lambda = \dot{\Lambda} = 0\}$ is not an invariant set when $s \neq 0$.

PROOF This corollary is proved by seeking a contradiction and assume that the set $\{\Lambda | \Lambda = \dot{\Lambda} = 0\}$ is an invariant set.

Taking the time derivative of Λ, one obtains

$$\dot{\Lambda} = \begin{bmatrix} (c\alpha_1 - \alpha_3)\dot{\Omega}_y + \alpha_3\alpha_1\tau_{ry} \\ (c\alpha_2 + \alpha_3)\dot{\Omega}_x - \alpha_3\alpha_2\tau_{rx} \end{bmatrix} \quad (24)$$

with $\tau_{rx} = -\dot{h}_x$ and $\tau_{ry} = -\dot{h}_y$ since $\tau_s = 0$ according to the definition of τ_s in (20b) and x^+ in (23).

Considering system in (9) and substituting controllers in (16) and (24) is further written as

$$\dot{\boldsymbol{\Lambda}} = \begin{bmatrix} \pi_1 + \alpha_3 \alpha_1 a_1 \\ \pi_2 - \alpha_3 \alpha_1 a_2 \end{bmatrix} \qquad (25)$$

with

$$\begin{bmatrix} \pi_1 \\ \pi_2 \end{bmatrix} =$$
$$\begin{bmatrix} (c\alpha_1 - \alpha_3)\left(-k_3\tilde{\Omega}_y + \dot{\Omega}_{dy}\right) + \alpha_3\left(-k_3\tilde{\Omega}_x + \dot{\Omega}_{dx}\right) \\ (c\alpha_2 + \alpha_3)\left(-k_3\tilde{\Omega}_y + \dot{\Omega}_{dy}\right) - \alpha_3\left(-k_3\tilde{\Omega}_y + \dot{\Omega}_{dy}\right) \end{bmatrix}.$$
$$(26)$$

Notice that Ω_z cannot stay at zero when $s \neq 0$, and $a_1 = [(J_y - J_z)\Omega_y + h_y]\Omega_z$, $a_2 = [(J_z - J_x)\Omega_x - h_x]\Omega_z$, one can conclude that the terms in square bracket of a_1 and a_2 must be equal to zero such that $\dot{\boldsymbol{\Lambda}} = 0$ is possible to be true for arbitrary Ω_z.

Multiplying $\alpha_2\alpha_3$ and $\alpha_1\alpha_3$ to $(J_y - J_z)\Omega_y + h_y$ and $(J_z - J_x)\Omega_x - h_x$, respectively, one obtains

$$(\alpha_3 - \alpha_2)\Omega_y + \alpha_2\alpha_3 h_y = 0 \qquad (27a)$$
$$(\alpha_1 - \alpha_3)\Omega_x - \alpha_1\alpha_3 h_x = 0. \qquad (27b)$$

When $\|\boldsymbol{\Lambda}\| = 0$, one also has

$$(c\alpha_1 - \alpha_3)\,\Omega_y - \alpha_3\alpha_1 h_y = 0 \qquad (28a)$$
$$(c\alpha_2 + \alpha_3)\,\Omega_x + \alpha_3\alpha_2 h_x = 0. \qquad (28b)$$

Solving h_x and h_y using (28a) and (28b) and substituting them into (27a) and (27b), it gives

$$[\alpha_2\,(\alpha_1 - \alpha_3) + \alpha_1\,(c\alpha_2 + \alpha_3)]\,\Omega_x = 0 \qquad (29a)$$
$$[\alpha_1\,(\alpha_3 - \alpha_2) + \alpha_2\,(c\alpha_1 - \alpha_3)]\,\Omega_y = 0. \qquad (29b)$$

Since the zero coefficients should be independent of Ω_x and Ω_y, thus it gives

$$[\alpha_2\,(\alpha_1 - \alpha_3) + \alpha_1\,(c\alpha_2 + \alpha_3)] = 0 \qquad (30a)$$
$$[\alpha_1\,(\alpha_3 - \alpha_2) + \alpha_2\,(c\alpha_1 - \alpha_3)] = 0. \qquad (30b)$$

Minus (30b) from (30a), one obtains

$$2\alpha_1\alpha_2 = 0. \qquad (31)$$

However, $\alpha_1 = 1/J_x$, $\alpha_2 = 1/J_y$ with J_x and J_y being the principle moments of inertia along X and Y axes. Physically, J_x and J_y cannot be zero. This physical property contradicts (31) and the assumption is wrong. Hence, the set $\{\boldsymbol{\Lambda}|\boldsymbol{\Lambda} = \dot{\boldsymbol{\Lambda}} = 0\}$ is not an invariant set. ∎

THEOREM 3 Consider relative dynamic (9) and let (20) be the controller, s converges to zero in finite time and the settling time is given by $t_s \leq \frac{1}{k_5} \ln \frac{\sqrt{2k_5}\sqrt{V_3(x_0)} + k_7}{k_7}$.

PROOF With the denotation of α_1, α_2, α_3, and c, the system in (9) can be further simplified by substituting (20a) and (16)

$$\begin{cases} \dot{\Omega}_x = -k_3\tilde{\Omega}_x + \dot{\Omega}_{dx} + \alpha_1\tau_{sx} \\ \dot{\Omega}_y = -k_3\tilde{\Omega}_y + \dot{\Omega}_{dy} + \alpha_2\tau_{sy} \\ \dot{\Omega}_z = c\Omega_x\Omega_y + \alpha_3\Omega_y h_x - \alpha_3 h_y\Omega_x. \end{cases} \qquad (32)$$

A Lyapunov candidate is given by

$$V_3 = \frac{s^2}{2}. \qquad (33)$$

Taking the time derivative, one obtains

$$\dot{V}_3 = s\dot{s}$$
$$= s \begin{Bmatrix} k_4\left(c\Omega_x\Omega_y + \alpha_3\Omega_y h_x - \alpha_3 h_y\Omega_x\right) \\ + c\dot{\Omega}_x\Omega_y + c\Omega_x\dot{\Omega}_y + \alpha_3\dot{\Omega}_y h_x \\ - \alpha_3 h_y\dot{\Omega}_x + \alpha_3\Omega_y\dot{h}_x - \alpha_3\dot{h}_y\Omega_x \end{Bmatrix}. \qquad (34)$$

Notice that $\tau_x = -\dot{h}_x$ and $\tau_y = -\dot{h}_y$, (26) is further simplified by substituting (24)

$$\dot{V}_3 = s\left\{\Phi + \boldsymbol{\Lambda}^T \begin{bmatrix} \tau_{sx} \\ \tau_{sy} \end{bmatrix}\right\}. \qquad (35)$$

Substituting (20b) into (35) when $\|\boldsymbol{\Lambda}\| \neq 0$, one obtains

$$\dot{V}_3 = s\left[-k_5 s\boldsymbol{\Lambda}^T\boldsymbol{\Lambda}^+\right] - s\left[k_6\mathrm{sgn}(s)\boldsymbol{\Lambda}^T\boldsymbol{\Lambda}^+ + \Phi\right]$$
$$\leq -k_5 s^2 - k_7\,|s| \leq 0. \qquad (36)$$

When $\|\boldsymbol{\Lambda}\| = 0$, Corollary 1 states that the set $\{\boldsymbol{\Lambda}|\boldsymbol{\Lambda} = \dot{\boldsymbol{\Lambda}} = 0\}$ is not a invariant set. Thus, $\|\boldsymbol{\Lambda}\|$ will pass zero immediately. Then, the time trajectory of V_3 will be governed by (36).

According to the Lemma in (2), V_3 converges to zero in finite time and the settling time can be estimated by $t_s \leq \frac{1}{k_5} \ln \frac{\sqrt{2k_5}\sqrt{V_3(x_0)} + k_7}{k_7}$. ∎

In practical control, controller in (20a) is adopted to control the whole system. Theorem 3 states that s and Ω_z converges to zero in finite time. When $s = 0$, $\boldsymbol{\tau}_s$ becomes zero. Hence, controller (20a) turns to controller in (16). Under the controller in (16), designed Ω_{dx} and Ω_{dy} are achieved exponentially. Simultaneously, the relative error kinematic (14) is stabilized. Then, attitude maneuver is completed. Similar control approach can be found in [28] for the spacecraft attitude control using two thrusters.

REMARK 1 In (20b), the signum function is adopted. To improve the control performance, a smooth hyperbolic tangent, which can be regarded as the approximation of the signum function, is employed to replace the signum function.

REMARK 2 To avoid the discontinuity and the singularity caused by the operator in (23). A modification of this operator is given by:

$$\boldsymbol{\Lambda}^* = \frac{\boldsymbol{\Lambda}}{\boldsymbol{\Lambda}^T\boldsymbol{\Lambda} + |s|}. \qquad (37)$$

The mechanism can be found in [29]. Through this modification, simulations show acceptable results. However, the aforementioned theorem may or may not be rigorously retained.

After the modification, the overall controller (20a) and (20b) is given by

$$\boldsymbol{\tau} = -\left(k_5 s + k_6 \tanh(s)\right) \boldsymbol{\Lambda}^* + \begin{bmatrix} -a_1 + J_x \dot{\Omega}_{dx} - k_3 J_x \tilde{\Omega}_x \\ -a_2 + J_y \dot{\Omega}_{dy} - k_3 J_y \tilde{\Omega}_y \end{bmatrix}.$$
(38)

IV. NUMERICAL SIMULATION

In this section, numerical simulations are conducted to demonstrate the effectiveness of proposed controller.

A. Generalized Singular Robust Steering Law

Various steering laws have been proposed, such as the singularity avoidance steering law, singularity escape steering law, and the hybrid logic. Among these steering laws, the generalized singular robust steering law has been widely adopted in the spacecraft attitude control system due to its significant capability of escaping from any internal singularities [30]. The Jacobian matrix A as in (4) will lose rank when

$$\det(A) = \sin \delta_2 \cos \delta_1 - \sin \delta_1 \cos \delta_2 = 0.$$
(39)

To avoid the singularity, an auxiliary matrix E is defined as

$$E = \begin{bmatrix} 1 & \varepsilon \\ \varepsilon & 1 \end{bmatrix} > 0$$
(40)

with $\varepsilon = \varepsilon_0 \sin(\omega t + \phi)$.

Then, the gimbal angular velocity is determined by

$$\dot{\boldsymbol{\delta}} = -\frac{1}{h_0} A^T \left(A A^T + \lambda E\right)^{-1} \boldsymbol{\tau}$$
(41)

where $\lambda = \lambda_0 e^{-\mu \det(A A^T)}$.

The parameters are chosen as $\varepsilon = 0.01 \sin(0.05\pi t + 0.5\pi)$, $\lambda_0 = 0.01$, and $\mu = 10$.

B. Simulation Results

A practical 320-kg minisatellite UoSAT-12, as in [21], is chosen to show the effectiveness of the proposed control law with

$$J_x = 40.45, \ J_y = 42.09, \ J_z = 42.36 \ \left(\text{kg} \cdot \text{m}^2\right).$$

The CMGs are chosen with a constant angular momentum $h_0 = 0.347$ N·m·s. The maximum gimbal angular velocity is set to $90°/s$.

In the simulation, k_1 is the slope of the linear switching line in the $\Omega - e_v$ plane (similar to the phase plane) and k_2 is a gain for nonlinear term in (15). They are chosen as $k_1 = 0.01$ and $k_2 = 0.08$, as in [21]. k_3 is the inverse of the time constant of the rate error control. It is chosen as $1/k_3 = 20$ s. k_4 appears in the sliding mode surface for Ω_z and $\hat{\Omega}_z$ [see (19)]. It is used to govern the system performance on the sliding surface and chosen as $k_4 = 11$. k_5 and $k_6 = \|\Phi\| + k_7$ are the feedback gains of s and $\text{sign}(s)$ to guarantee the finite-time convergence [see (20b)]. Thus, k_5 and k_7 are used to govern the reaching process and chosen to be $k_5 = 4$ and $k_7 = 0.1$.
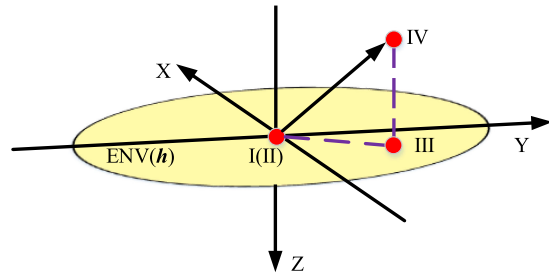

Fig. 3. Relationship of the angular momentum of listed scenarios and momentum envelope of the CMG array (Note: Illustration of four different initial angular momentum when only two parallel SGCMGs are available for attitude control, where the yellow circular disk, i.e., ENV($\boldsymbol{h}$), is the momentum envelope of two SGCGMs. The arrow here stands for the initial angular momentum of the Case IV, which lies outside of the circular momentum disk.).

As stated in (1), the angular momentum of the CMG array is constrained in the X–Y plane. The vector $R(Q_d)R(Q_0)^T h_t$ is denoted as $\hbar$. The feasibility requires the third row of $\hbar$ to be zero rather than h_t. In reverse, $h_t = 0$ guarantees $\hbar = 0$ and it is just a general solution of $\hbar = 0$. Thus, the zero momentum assumption is a sufficient condition and it is too conservative. In this correspondence, four scenarios, including three feasible attitude combinations and an additional infeasible condition listed in Table I shown in Fig. 3, are conducted. Case I corresponds to a rest-to-rest maneuver, where the initial angular velocity is set to be zero. The initial angular momentum of the CMG array is set to be $\delta_1 = 0$ and $\delta_1 = \pi$, respectively. In Case II, the angular momentums of the two CMGs are perpendicular. Then, angular velocity of the spacecraft is chosen as $\omega_x = -h_0/J_x$ and $\omega_y = -h_0/J_y$ such that the angular momentum of CMG spacecraft is zero. The initial angular momentums of CMG spacecraft in both Case I and Case II are zero and they correspond to the origin in the momentum envelop, as shown in Fig. 3. In such cases I and II, arbitrary attitude can be achieved and most of existing works focus on studying Cases I and II. However, except for the origin, i.e., Cases I and II, the states lying inside the momentum envelope (the points on the circular disk) are also feasible/achievable. Case III shows such situations with $\hbar_z = 0$. Comparing to the cases under zero angular momentum assumption, Case III contains the vast majority of feasible/achievable attitude. Thus, our research work and results here extensively enlarge the controllable initial conditions compared to existing studies, i.e., Cases I and II, and greatly improve the attainable control system possibilities for the problem of "underactuated attitude maneuver using two parallel single-gimbal control moment gyros." Case IV shows an infeasible condition under which $\hbar_z \neq 0$. Even though such cases are infeasible, the spacecraft will be control to be a periodic oscillation in the vicinity of the equilibrium. Detailed results are shown in Figs. 4–7.

1) *Case I. Rest-to-Rest Maneuver:* Rest-to-rest maneuver is conducted and the simulation results are shown in Fig. 4. Fig. 4(a) shows that the quaternion error converges

TABLE I
Initial Condition for the Simulation Senarios

Case No.	Q_{0v}	Q_{dv}	ω_0 [deg/s]	h_t [Nms]	δ_0
Case I	$[0,\ 0,\ 0]^T$	$[-0.7,\ 0.01,\ 0.3]^T$	$[0,\ 0,\ 0]^T$	$[0,\ 0,\ 0]^T$	$[0,\ \pi]^T$
Case II	$[-0.4,\ 0.2,\ 0]^T$	$[-0.7,\ 0.01,\ 0.3]^T$	$[-0.4915,\ -0.4724,\ 0]^T$	$[0,\ 0,\ 0]^T$	$[0,\ \pi/2]^T$
Case III	$[0.5,\ 0.5,\ 0.5]^T$	$[-0.5\ -0.5,\ -0.5]^T$	$[0,\ -0.35,\ 0.4]^T$	$[0,\ -0.2571,\ 0.2957]^T$	$[0,\ \pi]^T$
Case IV	$[0.5,\ 0.5,\ 0.5]^T$	$[-0.5\ -0.5,\ -0.5]^T$	$[-0.05,\ -0.35,\ 0.4]^T$	$[-0.0353,\ -0.2571,\ 0.2957]^T$	$[0,\ \pi]^T$

Note: The scalar part of $\boldsymbol{Q}_{0v}$ and $\boldsymbol{Q}_{0v}$ is calculated by $Q_{00} = \sqrt{1 - \boldsymbol{Q}_{0v}^T\boldsymbol{Q}_{0v}}$ and $Q_{d0} = \sqrt{1 - \boldsymbol{Q}_{dv}^T\boldsymbol{Q}_{dv}}$.
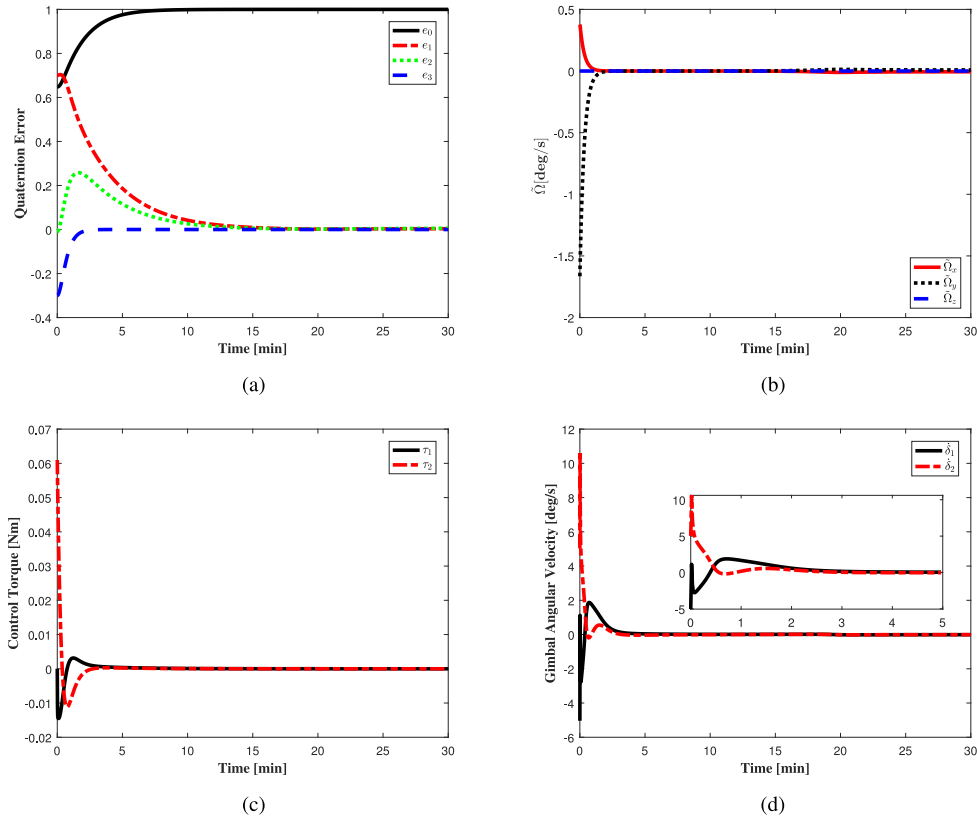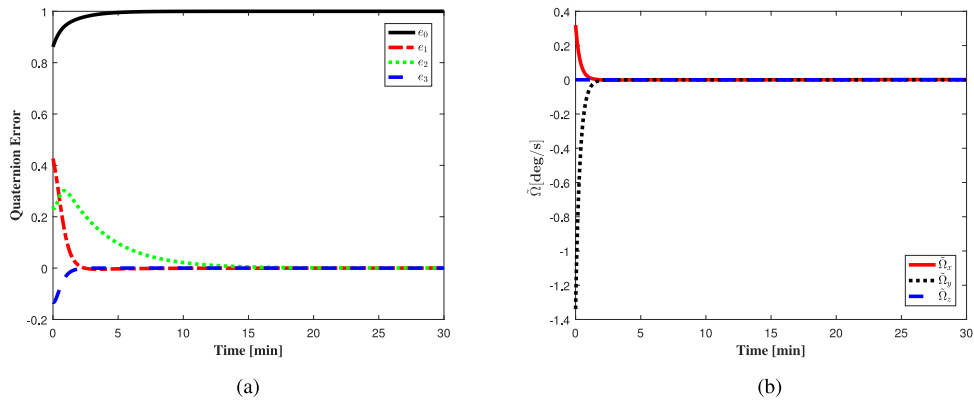

Fig. 4. Control results of Case I. (a) Quaternion error. (b) Angular velocity error. (c) Control torque. (d) Gimbal angular velocity.

to zero gradually, which states that the attitude maneuver is completed. Fig. 4(b) shows the difference between the velocity $\boldsymbol{\Omega}$ and the desired value $\boldsymbol{\Omega}_d$. The error $\tilde{\boldsymbol{\Omega}}$ converges to zero within 5 min. Combining Fig. 4(a) and (b), it can be concluded that the desired angular velocity $\boldsymbol{\Omega}_d$ is tracked. Fig. 4(c) shows the control torque that is smaller than 70 mN·m. Fig. 4(d) gives the history of gimbal angular velocity, which is far from the maximum angular velocity constraint $\pi/2$.

2) *Case II. Zero Angular Momentum Maneuver:* The simulation results of Case II, shown in Fig. 5, are quite similar to that shown in Fig. 4. Comparing to Case I, a different initial attitude and different initial angular velocity are chosen. Then, the initial quaternion error [see Fig. 5(a)] and initial velocity error $\tilde{\boldsymbol{\Omega}}$ [see Fig. 5(b)] are all different. A nonzero angular velocity is stabilized. Together with Case I, it can be concluded that an arbitrary rest attitude can be achieved with the utilization of the proposed control

law when the total angular momentum of CMG spacecraft is zero.

3) *Case III. Feasible Attitude Maneuver:* Fig. 6 demonstrates a feasible attitude maneuver. These feasible conditions are the complement of the zero angular momentum cases in the momentum envelope. The quaternion error is shown in Fig. 6(a). It can be seen that the attitude maneuver is achieved in 20 min, which is longer than the previous results. The attitude trajectory in Fig. 6(b) is much more complicated comparing to the previous ones with zero angular momentum. The complexity may come from the sliding mode control part to stabilize the angular velocity along the axis without direct input. Finally, the final orientation coincides with the target orientation. Fig. 6(c) and (d) shows the angular velocity tracking error and angular velocity trajectory. It can be seen that both the nonzero velocity tracking error and the angular velocities along three axes converge to zero within 20 min. Similarly, $\boldsymbol{\Omega}_d$ is first tracked

(a)

(b)

Fig. 5.   Control results of Case II. (a) Quaternion error. (b) Angular velocity error.

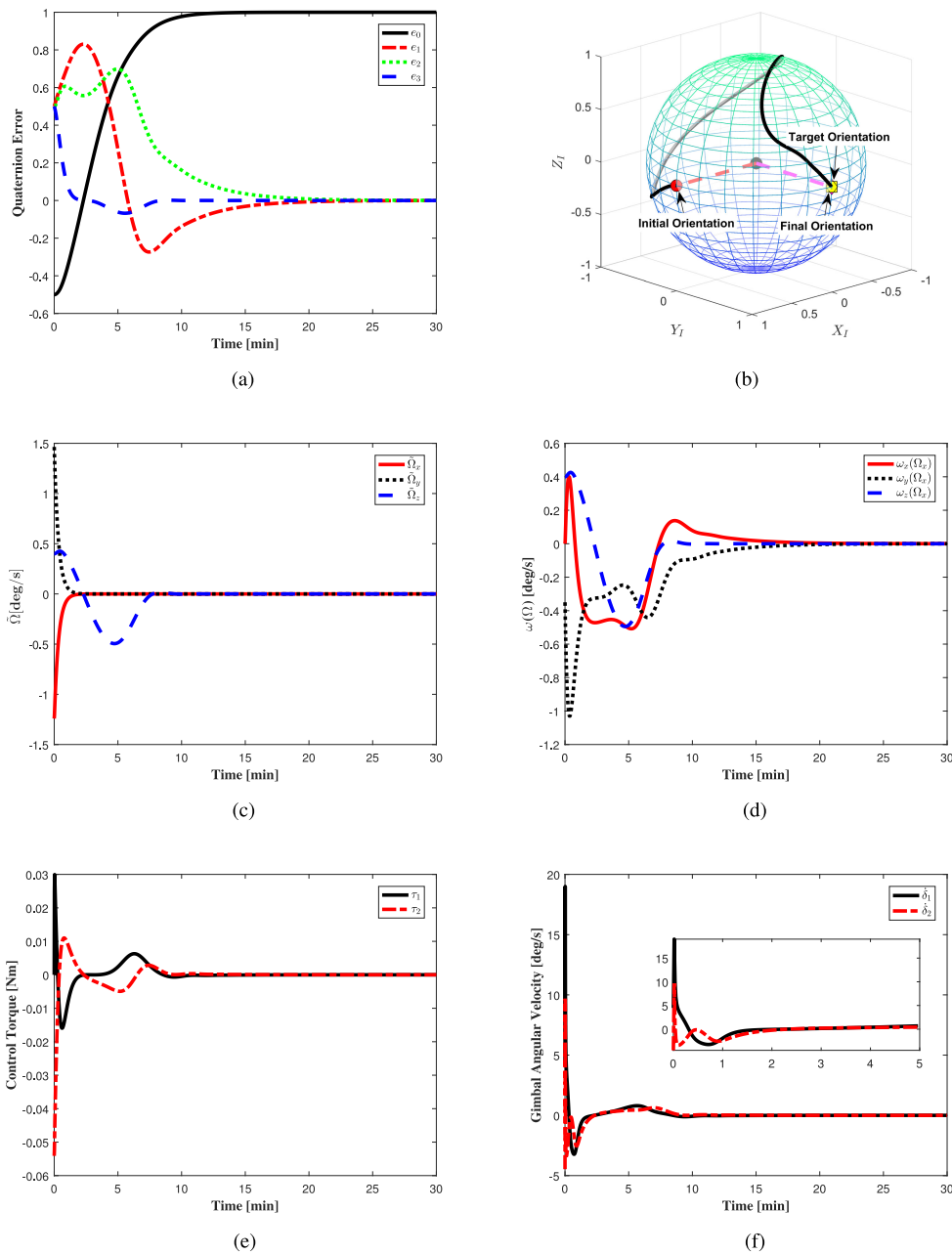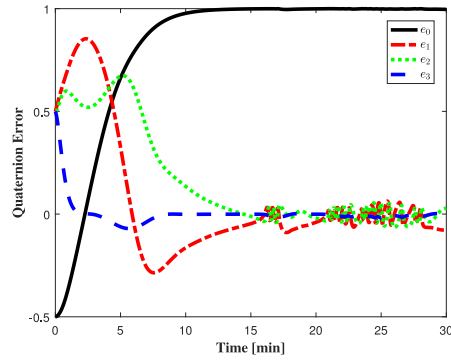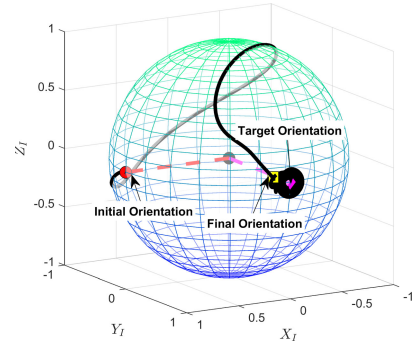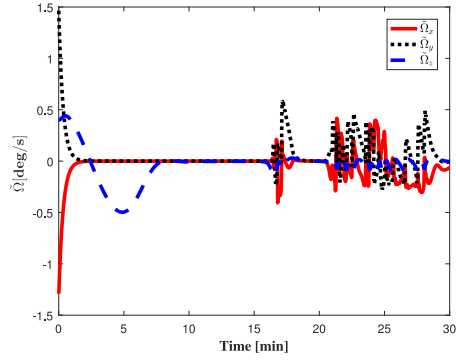(a)

(b)

(c)

(d)

(e)

(f)

Fig. 6.   Control results of Case III. (a) Quaternion error. (b) Attitude trajectory. (c) Angular velocity error. (d) Angular velocity. (e) Control torque.
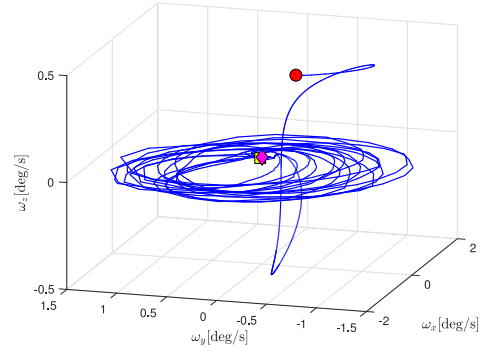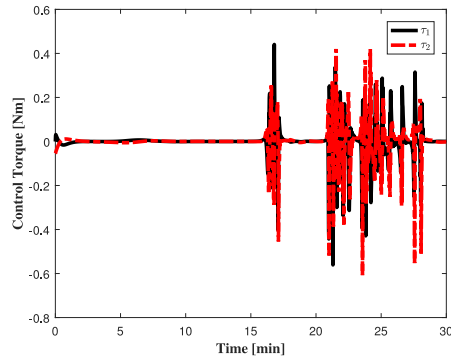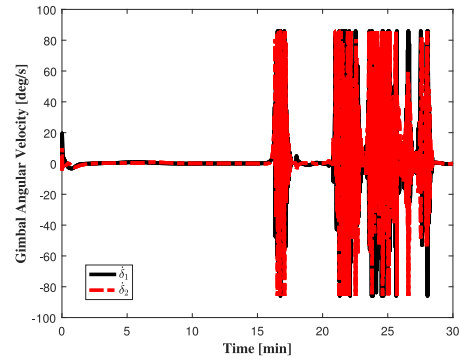(f) Gimbal angular velocity.
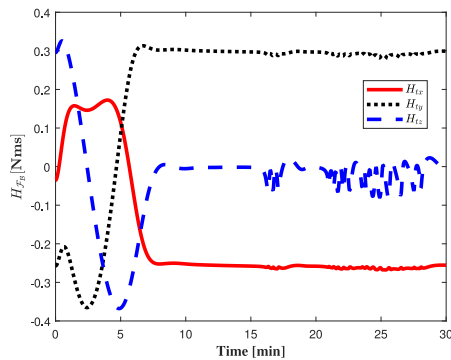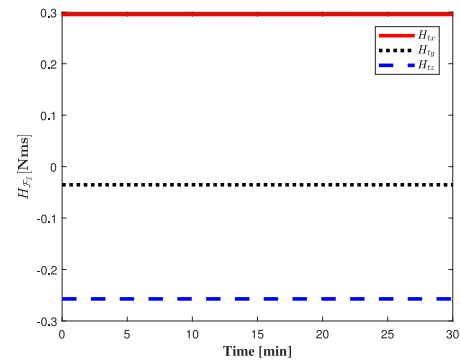
Fig. 7. Control results of Case IV. (a) Quaternion error. (b) Attitude trajectory. (c) Angular velocity error. (d) Angular velocity in 3-D space. (e) Control torque. (f) Gimbal angular velocity. (g) Angular momentum in $\mathcal{F}_B$. (h) Angular momentum in $\mathcal{F}_I$.

and then $\mathbf{\Omega}$ is stabilized. Fig. 6(e) and (f) demonstrates the control torque and gimbal angular velocity that are achievable using the CMGs.

Cases I–III give the simulation results using the proposed controller (38) when $e_1^2 + e_2^2 \neq 0$. The combination of theses three cases take up the vast majority of the feasible orientation.

4) Case IV. Infeasible Attitude Maneuver: On contrary to the feasible combinations, the cases when the angular momentum exceeds the angular momentum envelope are infeasible. In this case, the projection of the angular momentum on the envelop disk is the same as that of Case III and a nonzero extra component is added. Fig. 7 shows the results.

In Fig. 7(a), the quaternion error oscillates within a tube around the equilibrium. Fig. 7(b) presents the attitude trajectory. It is clear that the finial orientation does not coincide with the target orientation. But the trajectory tells that the spacecraft rotates around the target orientation in the adjacent region. This proves that the target attitude is a global attractor and the spacecraft is forced to get close to the target attitude. The oscillation in Fig. 7(a) corresponds to the repeated circular trajectory in Fig. 7(b). Fig. 7(c) illustrates the trajectory of the angular velocity tracking error. At the very beginning, the tracking error converges to the desired value. This phase can be regarded that the attraction of the target attitude is more effective. When the attitude gets close to the equilibrium, the influence caused by the obstacle of angular momentum conservation overweighs the attraction of the target attitude. Then, the tracking error starts to oscillate. Fig. 7(d) gives a 3-D angular velocity trajectory. The initial state is marked with circle and the final state is marked with square. It can be clearly observed that the angular velocity component along the Z-axis where there is no direct input is stabilized. This expands the controllable conditions enormously compared to the existing works where ω_z is assumed zero. Fig. 7(e) and (f) shows the control torque and gimbal angular velocity, respectively. To show the angular momentum conservation property, the angular momentum in both the body frame and inertial frame are shown in Fig. 7(g) and (h), respectively. Clearly, it is conserved in the inertial frame. Similarly, the conservation property holds for Cases I–III.

V. CONCLUSION

This correspondence investigates the underactuated attitude maneuver problem using two parallel control moment gyros. A systematic closed-loop control solution is given. The proposed attitude controller is realized by a two-level control strategy. First, the angular velocity along the axis without direct input is assumed zero. An ideal relative kinematic stabilizer and desired relative angular velocity tracker are designed for the reduced relative dynamics and kinematics. Second, a higher level sliding mode control law is proposed to stabilize the nonzero angular velocity, which is assumed to be zero in the previous design with a sufficient utilization of the coupling effect of the relative dynamics. Simulation results show that the target attitude is a global attractor. The spacecraft can be controlled to the target attitude when the controllability condition is satisfied or the orientations are feasible. When the initial angular momentum exceeds that of CMG array, the spacecraft can also be forced to rotate around the target orientation in the adjacent region.

CHENGFEI YUE
Institute of Space Science and Applied Technology, Harbin Institute of Technology, Shenzhen, China

FAN WU
FENG WANG
XIBIN CAO
Research Center of the Satellite Technology, Harbin Institute of the Technology, Harbin, China

QIANG SHEN
Shanghai Jiao Tong University, Shanghai, China

KRISHNA DEV KUMAR
Ryerson University, Toronto, Canada

REFERENCES

[1] C.-Y. Li, W.-X. Jing, and C.-S. Gao
Adaptive backstepping-based flight control system using integral filters
Aerosp. Sci. Technol., vol. 13, no. 2-3, pp. 105–113, 2009.

[2] M. Yu and C. Li
Robust adaptive iterative learning control for discrete-time nonlinear systems with time-iteration-varying parameters
IEEE Trans. Syst., Man, Cybern.: Syst., vol. 47, no. 7, pp. 1737–1745, Jul. 2017.

[3] S. Yin, B. Xiao, S. X. Ding, and D. Zhou
A review on recent development of spacecraft attitude fault tolerant control system
IEEE Trans. Ind. Electron., vol. 63, no. 5, pp. 3311–3320, May 2016.

[4] Q. Shen, C. Yue, C. H. Goh, and D. Wang
Active fault-tolerant control system design for spacecraft attitude maneuvers with actuator saturation and faults
IEEE Trans. Ind. Electron., vol. 66, no. 5, pp. 3763–3772, May 2019.

[5] Q. Shen, D. Wang, S. Zhu, and E. K. Poh
Integral-type sliding mode fault-tolerant control for attitude stabilization of spacecraft
IEEE Trans. Control Syst. Technol., vol. 23, no. 3, pp. 1131–1138, May 2015.

[6] B. Xiao and S. Yin
Velocity-free fault-tolerant and uncertainty attenuation control for a class of nonlinear systems
IEEE Trans. Ind. Electron., vol. 63, no. 7, pp. 4400–4411, Jul. 2016.

[7] J. Jiang and X. Yu
Fault-tolerant control systems: A comparative study between active and passive approaches
Annu. Rev. Control, vol. 36, no. 1, pp. 60–72, 2012.

[8] A. Choukchou-Braham, B. Cherki, M. Djemaï, and K. Busawon
Analysis and Control of Underactuated Mechanical Systems.
Berlin, Germany: Springer, 2013.

[9] L. Jin and S. Xu
Underactuated spacecraft angular velocity stabilization and three-axis attitude stabilization using two single gimbal control moment gyros
Acta Mechanica Sinica, vol. 26, no. 2, pp. 279–288, 2010.

[10] P. Crouch
Spacecraft attitude control and stabilization: Applications of geometric control theory to rigid body models
IEEE Trans. Autom. Control, vol. 29, no. 4, pp. 321–331, Apr. 1984.

[11] J. Li, C. Gao, C. Li, and W. Jing
A survey on moving mass control technology
Aerosp. Sci. Technol., vol. 82, pp. 594–606, 2018.

[12] J. Li, S. Chen, C. Li, C. Gao, and W. Jing
Adaptive control of underactuated flight vehicles with moving mass
Aerosp. Sci. Technol., vol. 85, pp. 75–84, 2019.

[13] F. Boyer and M. Alamir
Further results on the controllability of a two-wheeled satellite
J. Guid., Control, Dyn., vol. 30, no. 2, pp. 611–619, 2007.

[14] S. P. Bhat and P. K. Tiwari
Controllability of spacecraft attitude using control moment gyroscopes
IEEE Trans. Autom. Control, vol. 54, no. 3, pp. 585–590, Mar. 2009.

[15] T. Sasaki, T. Shimomura, and S. Kanata
Gain-scheduled control and singularity avoidance with a double-gimbal variable-speed control moment gyro
In *Proc. AIAA/AAS Astrodyn. Specialist Conf.*, 2016, pp. 2016–5370.

[16] S. Kasai, H. Kojima, and M. Satoh
Spacecraft attitude maneuver using two single-gimbal control moment gyros
Acta Astronaut., vol. 84, pp. 88–98, 2013.

[17] P. Tsiotras *et al.*
Control of spacecraft subject to actuator failures- state-of-the-art and open problems
J. Astronaut. Sci., vol. 48, no. 2, pp. 337–358, 2000.

[18] H. Gui, G. Vukovich, and S. Xu
Attitude stabilization of a spacecraft with two parallel control moment gyroscopes
J. Guid., Control, Dyn., vol. 39, no. 3, pp. 728–735, 2016.

[19] H. Gui, L. Jin, S. Xu, and J. Zhang
On the attitude stabilization of a rigid spacecraft using two skew control moment gyros
Nonlinear Dyn., vol. 79, no. 3, pp. 2079–2097, 2015.

[20] C. Yue, K. D. Kumar, Q. Shen, C. H. Goh, and T. H. Lee
Attitude stabilization using two parallel single-gimbal control moment gyroscopes
J. Guid., Control, Dyn., vol. 42, no. 6, pp. 1353–1364, 2019.

[21] N. M. Horri, P. Palmer, and S. Hodgart
Practical implementation of attitude-control algorithms for an underactuated satellite
J. Guid., Control Dyn., vol. 35, no. 1, pp. 40–50, 2012.

[22] B. Wie
Singularity analysis and visualization for single-gimbal control moment gyro systems
J. Guid. Control Dyn., vol. 27, no. 2, pp. 271–282, 2004.

[23] K. Yamada, I. Jikuya, and O. Kwak
Rate damping of a spacecraft using two single-gimbal control moment gyros
J. Guid., Control, Dyn., vol. 36, no. 6, pp. 1606–1623, 2013.

[24] A. Tayebi
Unit quaternion-based output feedback for the attitude tracking problem
IEEE Trans. Autom. Control, vol. 53, no. 6, pp. 1516–1520, Jul. 2008.

[25] A.-M. Zou, K. D. Kumar, Z.-G. Hou, and X. Liu
Finite-time attitude tracking control for spacecraft using terminal sliding mode and Chebyshev neural network
IEEE Trans. Syst., Man, Cybern., Part B (Cybern.), vol. 41, no. 4, pp. 950–963, Aug. 2011.

[26] S. Yu, X. Yu, B. Shirinzadeh, and Z. Man
Continuous finite-time control for robotic manipulators with terminal sliding mode
Automatica, vol. 41, no. 11, pp. 1957–1964, 2005.

[27] S. Sastry
Nonlinear Systems: Analysis, Stability, and Control, vol. 10. Berlin, Germany: Springer, 2013.

[28] A.-M. Zou, K. D. Kumar, and A. H. J. de Ruiter
Spacecraft attitude control using two control torques
Inf. Sci., vol. 408, pp. 23–40, 2017.

[29] A. H. Bajodah
Asymptotic perturbed feedback linearisation of underactuated Euler's dynamics
Int. J. Control, vol. 82, no. 10, pp. 1856–1869, 2009.

[30] B. Wie, D. Bailey, and C. Heiberg
Singularity robust steering logic for redundant single-gimbal control moment gyros
J. Guid., Control, Dyn., vol. 24, no. 5, pp. 865–872, 2001.

CORRESPONDENCE